Determination of Binding Strengths of a Host−Guest Complex Using Resonance Raman Scattering

Edward H. Witlicki,[†] Stinne W. Hansen,[‡] Martin Christensen,[‡] Thomas S. Hansen,[‡] Sune D. Nygaard,[‡] Jan O. Jeppesen,[‡] Eric W. Wong,[§] Lasse Jensen,[||] and Amar H. Flood*[,†]

Chemistry Department, Indiana University, 800 East Kirkwood Avenue, Bloomington, Indiana 47405, Department of Physics and Chemistry, University of Southern Denmark, Odense University, Campusvej 55, 5230 Odense M, Denmark, Atomate Corporation, 2665-D Park Center Drive, Simi Valley, California 93065, and Department of Chemistry, The Pennsylvania State University, 104 Chemistry Building, University Park, Pennsylvania 16802

Received: June 3, 2009; Revised Manuscript Received: July 9, 2009

The detection of analyte-binding events by receptors is drawing together the fields of Raman spectroscopy and supramolecular chemistry. This study is intended to facilitate this cohering by examining a model system in the solution phase. The resonance Raman scattering (RRS) spectra of the complexation between tetrathiafulvalene (TTF) and cyclobis(paraquat-*p*-phenylene) ($CBPQT^{4+}$) has been used as the model to characterize the binding event of a host−guest system. RRS spectra are generated by excitation ($\lambda_{exc} = 785$ nm) within the lowest-energy charge-transfer (CT) transition ($\lambda_{max} = 865$ nm) of the TTF⊂$CBPQT^{4+}$ complex. The paired binding curves from the RRS and UV−vis−NIR titration data agrees with prior work, and a ΔG of -5.7 ± 0.6 kcal mol^{-1} (MeCN, 298 K) was obtained for the complexation of TTF with $CBPQT^{4+}$. Computations on the complex and its components reproduce the energy shifts and resonance enhancements of the Raman band intensities, providing a basis to identify the structural and vibrational changes occurring upon complexation. The changes in bond lengths coincide with partial depopulation of a TTF-based HOMO and population of a $CBPQT^{4+}$-based LUMO through CT mixing in the ground state of $0.46e^-$. The structural changes upon complexation generally lead to lower wavenumber vibrations and to changes in the normal mode descriptions.

Introduction

Molecule-based approaches to sensing[1] leverage the lessons and practices of host−guest chemistry.[2] Ideally, (1) strong and selective binding (2) triggers a change in an optical[1] or an electrical response.[3] Solution-phase Raman spectroscopy is not usually among these optical techniques on account of its weak scattering cross section. Therefore, surface-enhanced Raman scattering (SERS)[4,5] is often used to enhance the Raman signals. The majority of these studies[6,7] that aim to quantify analyte−receptor binding make use of well-known receptors, such as, crown ethers,[6d] calixarenes,[6f,k,7g] cyclodextrins,[6h,7a] and resorcinarenes.[7c] However, the majority of all receptors presently being designed for binding with specific analytes are focused on solution-phase detection.[1a,8] To facilitate the use of such designer receptors for SERS, it is therefore beneficial to first understand the binding event in solution. To this end, it was a surprise to discover that the use of Raman scattering to quantify binding events in solution is comparatively rare,[9,10] even though its use as a structural tool is more common.[11] Consequently, the purpose of this study is to aid in expanding the use of Raman spectroscopy into the field of supramolecular chemistry by utilizing a model host−guest complex (Scheme 1a).

Prior Studies Using Raman Spectroscopy to Quantify Binding Constants. There are only two prior examples that use Raman spectroscopy to measure solution-phase binding constants (Scheme 1b). The first[9] characterizes the heterodimerization strengths between a range of electron donors and the acceptor tetracyanoethylene (TCNE). The second measures axial binding of *N*-heterocyclic bases (pyridine, 2-, 3-, and 4-picolene) to zinc(II) *meso*-tetraphenylporphyrin (ZnTPP).[10] Neither of these represents molecular recognition of a guest by a host. Where host−guest complexation has been the topic of study,[11] the Raman spectroscopy was employed to provide information on the bonding and structure of the resulting complex. In these cases, the association strength is usually established using more standard techniques, for example, ^{1}H NMR and UV−vis−NIR spectroscopic titrations.

General Design Criteria for Measuring Binding Constants of Host−Guest Complexes. Compared with Raman spectroscopy, the numbers of quantitative ^{1}H NMR and UV−vis−NIR spectroscopic studies are far larger, and there are more models of binding available for data analysis. One reason for the large difference stems from the more straightforward experimental design. In general, the disassociation constant, $K_d = 1/K_a$, determines[12] the ideal concentration region in which a host−guest titration is conducted. This concentration ($\approx K_d$/M) therefore dictates the technique to use: ^{1}H NMR for $K_a = 10$ to 10^3 M^{-1} ($K_d = 1$ M to 1 mM) and UV−vis−NIR spectroscopy for $K_a = 10^3$ to 10^6 M^{-1} ($K_d = 1$ mM to 1 μM). For Raman spectroscopy experiments, the design criteria are additionally dependent on the details of the supramolecular system. The more familiar normal Raman scattering, which is frequently introduced as a

* Corresponding author.
[†] Indiana University.
[‡] University of Southern Denmark.
[§] Atomate Corporation.
[||] The Pennsylvania State University.

10.1021/jp905202x CCC: $40.75
Published on Web 07/31/2009

SCHEME 1: (a) Model Complex Characterized Herein between Tetrathiafulvalene (TTF) and Cyclobis(paraquat-*p*-phenylene) ($CBPQT^{4+}$) and (b) Two Prior Examples of Using Resonance Raman Spectroscopy to Quantify Binding Constants: TCNE and Hexamethylbenzene Heterodimers[9] and Axial Binding of Pyridine to ZnTPP[10]

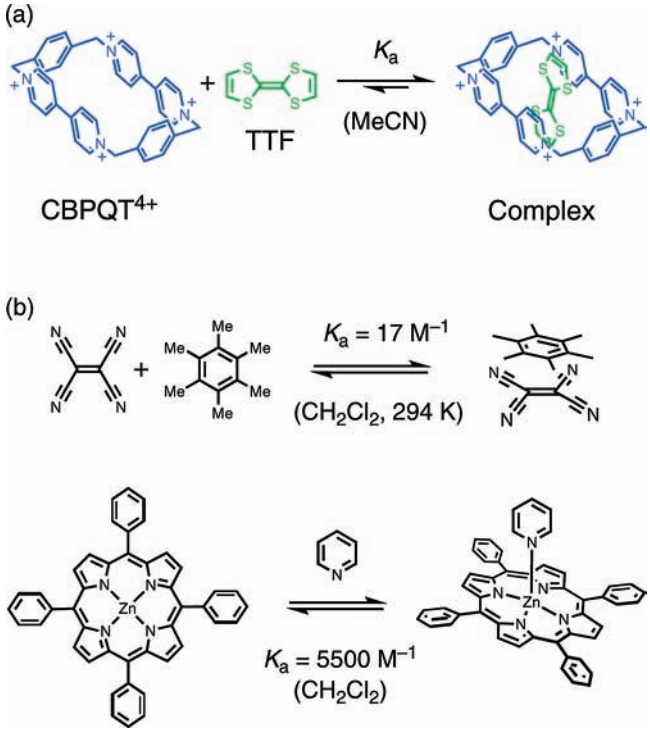

complement to FTIR spectroscopy, is a weak phenomenon.[13] In this case, ~1 mM is an approximate lower concentration limit when making use of modern instrumentation.[14] Another form of Raman scattering, and the one useful for TCNE[9] and ZnTPP,[10] is accessed when the laser excitation wavelength can be selected to coincide with a molecular or supramolecular chromophore, giving rise to resonance Raman scattering (RRS) with attendant signal enhancements of × 10 to 10^6.[15] For example, the low concentration used with ZnTPP (50 μM) is commensurate with both a moderate binding constant (K_a = 5500 M^{-1}) and the benefits of a large enhancement factor stemming from resonance using a laser excitation wavelength (λ_{exc}) of 441.6 nm coincident with the intense Soret band at 427 nm ($\varepsilon \approx 500\,000$ M^{-1} cm^{-1}).[9,16] With this information in mind, the optimal conditions (and concentration, λ_{exc}) for Raman experiments in solution can be identified. For data analysis, the two prior examples[9,10] used the same 1:1 binding model that accounts for the intensities of the Raman bands originating from the uncomplexed host (or guest). Lastly, increased accessibility to Raman spectrometers and microscopes is opening up more opportunities to use this spectroscopic technique in routine settings.

Motivations for Use of Raman Spectroscopy with Supramolecular Chemistry. For Raman studies of supramolecular systems, the quantification of binding events is being driven by applications with SERS.[6,7] These include detecting and measuring small amounts of an analyte for sensing[5] as well as plasmonics,[17] imaging,[7g] and the study of interfacial processes.[18] Other applicable situations include the use of RRS to simplify complicated spectroscopic signatures (e.g., resonant with hemes in biological samples)[11e,19] and for noninvasive in situ monitoring of chemical processes.[6j]

From a structural perspective, the majority of Raman studies are motivated by the chemical information available from the vibrational spectra. This approach is similar to the use of FTIR and is complementary to ^{1}H NMR spectroscopy. For example, when the noncovalent interactions involve functional groups that are not NMR-active as in changes in amide carbonyls during hydrogen bonding.[11q,u] In a related way, RRS spectroscopy complements UV−vis−NIR spectroscopy by providing vibrational and structural signatures of the specific chromophore responsible for the absorption band. In particular, the intensity of the Raman bands can be correlated to the geometry of the complex in its photoexcited state.[20] Consequently, interest has been directed toward measuring excited-state properties[21] of π-stacked donor−acceptor heterodimers. Other studies have correlated association strengths with shifts in vibrational band positions upon dimerization.[22]

Theoretical Simulations of Resonance Raman Scattering. The physical insight described above can best be attained by comparing experiment with theoretical simulations of the RRS spectra, thereby providing an accurate normal mode description of the observed vibrational bands. Recent progress in electronic structure methods has enabled the direct calculation of RRS spectra of molecules using the independent-mode, displaced harmonic oscillator model.[23−29] Within this model, the RRS intensities can be calculated from the excited-state displacements using the short-time approximation,[23,24,29] the vibronic theory,[30,31,23,24] or Heller's time-dependent theory.[28,32−34] Alternatively, the RRS intensities can be calculated from geometrical derivatives of the real and imaginary frequency-dependent polarizabilities.[49] Recent work has highlighted the importance of vibronic effects,[24,29] solvent effects,[24,26] and multiple excited states[27,49] in the calculations of the RRS intensities.

Model System and Experimental Design. To increase the basic understanding of the Raman spectroscopy of host−guest complexes, a series of experimental and computational studies have been designed and conducted. For this purpose, a model system has been selected (Scheme 1a). The tetrathiafulvalene[35] (TTF) molecule serves as a guest to the cyclobis(paraquat-*p*-phenylene)[36] ($CBPQT^{4+}$) macrocyclic host, and these together form a well-known[37] donor−acceptor complex. The complex has a binding constant of $K_a \approx 12\,000$ M^{-1} (MeCN, 298 K), dictating an ideal concentration at which to perform a titration of ~100 μM. The resulting complex is colored green, which arises from a TTF-to-$CBPQT^{4+}$ charge-transfer (CT) transition centered at 865 nm ($\varepsilon \approx 3500$ M^{-1}) in the absorption spectrum. The emergence of this absorption band provides an opportunity to use RRS by selecting a readily available excitation wavelength of λ_{exc} = 785 nm. Here resonance affords two benefits. First, it enhances the intensity of the Raman scattering, thereby extending the viable concentration range into the submillimolar region, which is necessary for the medium strength of association. Beneficially, the use of a lower concentration dictates that the intensity of the normal Raman scattering from the empty host, $CBPQT^{4+}$, will be insignificant. This situation allows for the use of a familiar binding model originally developed for UV−vis−NIR spectroscopy.[38] The nonresonant wavelength of λ_{exc} = 514.5 nm was selected as a negative control for verifying that the intensities of the vibrational bands are increased by a resonance mechanism. Computations of the structures and of the vibrational spectra were undertaken. A good correlation between the spectra helps to confirm the accuracy of the calculated geometries and electronic structures. The computed normal mode descriptions of the vibrations ultimately provide information on the nature of the CT interaction in the ground state.

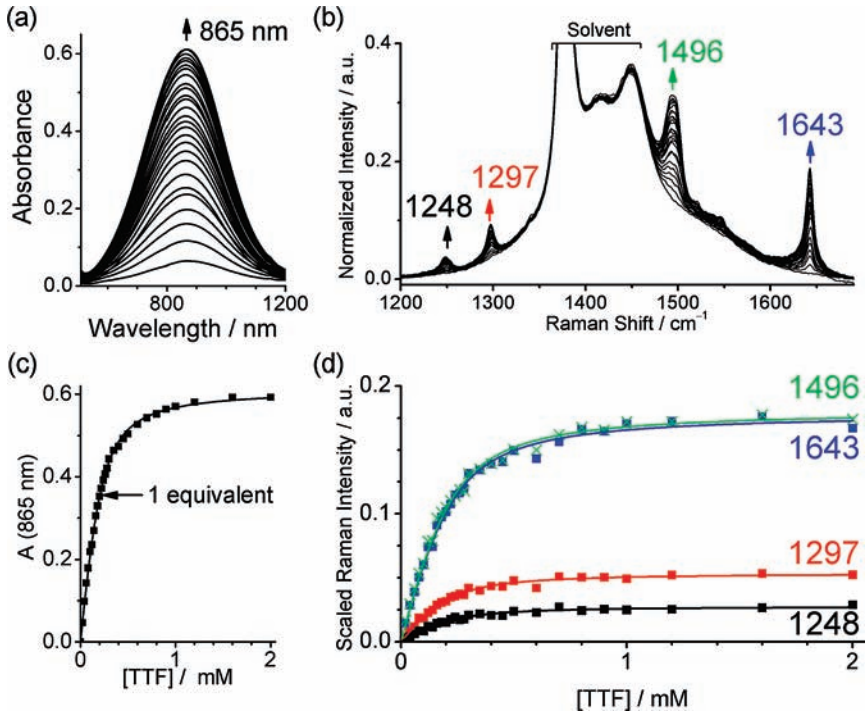

Figure 1. Titration of TTF into 200 μM $CBPQT^{4+}$ (MeCN, RT) as characterized by (a) UV−vis−NIR and (b) RRS (λ_{exc} = 785 nm) spectroscopy. Binding curves and their fits to a 1:1 model as obtained from the (c) UV−vis−NIR and (d) RRS spectra.

In this investigation, the binding constant obtained from fitting the resonance Raman data generated by the titration of TTF into $CBPQT^{4+}$ is found to concur with those obtained from more traditional UV−vis−NIR methods.[37] The RRS spectra generated computationally correlate well in the band positions and resonance enhancements. The calculated geometry changes that take place upon complexation are consistent with CT mixing among the frontier orbitals. Examination of the vibrations shows that some of the normal mode descriptions change significantly upon complexation. This finding emphasizes the importance of interpreting any observed changes in a band's shift and intensity with the aid of computation. Finally, the work outlined here can be directly extended to the characterization of other donor−acceptor host−guest complexes[39] and helps pave the way for other instances of molecular recognition.

Experimental Methods

General Methods. Solvents were purchased and purified using a PurSolv solvent purification system. TTF was purchased from Fluka (98%, HPLC grade) and used as received. Cyclobis(paraquat-*p*-phenylene) tetrakis(hexafluorophosphate) ($CBPQT\cdot 4PF_6$) was prepared according to literature procedures.[36] UV−vis−NIR measurements were collected using a Varian Cary 5000 spectrometer. The Raman spectra were recorded on an InVia Renishaw Raman Microscope with 785 nm excitation from a diode laser, and Raman shift positions were calibrated to the 520.5 cm^{-1} band of silicon. Laser powers were adjusted, and the acquisition times were extended in all cases to ensure an adequate signal-to-noise ratio. Spectra were baselined using Grams software (Thermo Galactic) where appropriate. Spectra for solid samples were recorded using a 50× numerical aperture (NA) = 0.7 objective lens focused down onto the samples spread out onto microscope slides. Solution state spectra were recorded using a 50×, NA = 0.7 long-working-distance objective lens focused into the MeCN solutions containing the sample inside a stoppered 1 mm path length quartz cuvette (Starna, type 21/Q/1, Spectrosil quartz). Short-acquisition-time spectra were recorded before and after long acquisitions to ensure no photodamage to the samples.

Raman Titration. In the typical procedure, a solution of TTF (10 mM) was prepared in anhydrous, Ar-purged CH_2Cl_2 such that in each of the aliquot volumes of ~2 μL was ~0.1 equiv. Aliquots of TTF were allowed to dry within gel-loading pipet tips using a 10 μL pipet. From 200 μL of a 1 mM $CBPQT^{4+}$ solution in anhydrous MeCN contained in a 1 mm quartz cuvette, the solution was drawn into a TTF-primed tip repeatedly until it was transferred completely. This approach was employed to remain in one solvent (MeCN) and to prevent dilution effects. On account of the TTF unit's propensity to oxidize, it is important to note that each tip was prepared immediately prior to use. Up to 10.0 equiv of TTF was added in this way to generate accurate binding isotherms.

Results and Discussion

Binding Constant Determination: Paired Resonance Raman and UV−vis−NIR Spectroscopy. The first step is to correlate the host−guest binding between TTF and $CBPQT^{4+}$ using RRS spectroscopy to more established techniques of characterization. Consequently, UV−vis−NIR spectra were recorded of the same solutions used for RRS spectra to generate paired data (Figure 1). The TTF was titrated into the solution as a solid using a tip-drying method, obviating the need to account for dilution. As expected, the 865 nm CT absorption band grows during the titration. The RRS spectra generated with 785 nm excitation are in resonance with the blue side of the CT transition. Initially (0 equiv TTF), the Raman spectrum is dominated by solvent scattering with a small $CBPQT^{4+}$ feature observed at 1650 cm^{-1}. Concomitantly, the $CBPQT^{4+}$-based bands of the complex located at 1643, 1297, and 1248 cm^{-1} grow in along with the TTF-based band at 1496 cm^{-1}.[40] These bands are shifted compared with the Raman bands of the uncomplexed TTF and $CBPQT^{4+}$ units (vide infra). On account

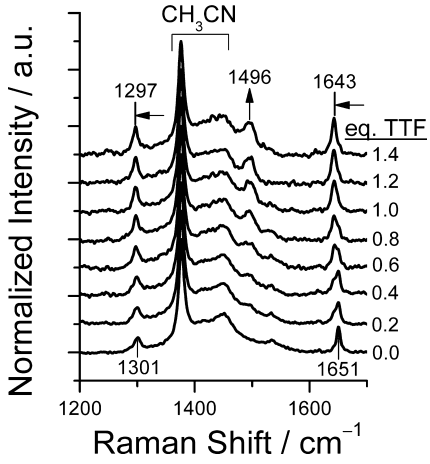

Figure 2. Raman titration data obtained off-resonance (λ_{exc} = 514.5 nm) by the addition of TTF to $CBPQT^{4+}$ in MeCN at 10 mM, 298 K.

of the fact that during the titration the concentration of $CBPQT^{4+}$ is constant and the high wavenumber vibration of $CBPQT^{4+}$ is only weakly seen at the beginning, the intensity of these Raman bands is enhanced by resonance with the CT transition. The same can be said for the TTF band on the basis of the fact that the Raman spectrum of free TTF at 0.1 mM (MeCN) is not detectable (Supporting Information).

To confirm the role of resonance enhancement, the Raman spectra recorded under nonresonant conditions with 514.5 nm excitation (Figure 2) show almost no change in the intensities of the $CBPQT^{4+}$ bands during the titration. Moreover, the scattering from these solutions is so weak that these spectra had to be recorded at 10 mM to see any reasonable signal. Consistent with the complexation event, the positions of the vibrational bands (λ_{exc} = 514.5 nm) reproduce the shifts seen from the RRS spectra (λ_{exc} = 785 nm).

TABLE 1: Summary of the Binding Constant Data Obtained from the Paired UV−vis−NIR and RRS Titration Data (200 μM $CBPQT^{4+}$, MeCN, 298 K)[a]

technique		method of fitting	ΔG/kcal mol^{-1}	K_a/M^{-1}
UV−vis-NIR	A (865 nm)	Drago	−5.7 ± 0.6	15 800
UV−vis-NIR	A (865 nm)	Sivvu	−5.8 ± 0.6	17 400
RRS	I (1643 cm^{-1})	Drago	−5.7 ± 0.6	15 000
RRS	I (1496 cm^{-1})	Drago	−5.7 ± 0.6	15 000
RRS	I (1297 cm^{-1})	Drago	−5.8 ± 0.6	18 000
RRS	I (1248 cm^{-1})	Drago	−5.7 ± 0.6	15 000

[a] Drago method adapted from ref 38; Sivvu method outlined in ref 43.

Binding curves (Figure 1) for the titration based on the RRS data mimic the one obtained from the UV−vis−NIR spectra. Both sets of data generate equal binding free energies (Table 1),[37] ΔG^{298} = −5.7 ± 0.6 kcal mol^{-1} (MeCN). The binding strength was previously measured using three different methods. From ^{1}H NMR spectroscopy (CD_3CN, 300 K) using the single-point method, it was −5.3 kcal mol^{-1}.[41] Using the dilution method by UV−vis−NIR spectroscopy (MeCN, 298 K), it was measured to be −5.5 kcal mol^{-1}.[41] Employing the method of isothermal titration microcalorimetry in MeCN (298 K), it was determined to be −5.27 ± 0.03 kcal mol^{-1}.[42] The values obtained by the spectroscopic titration methods used herein agree with these prior values.

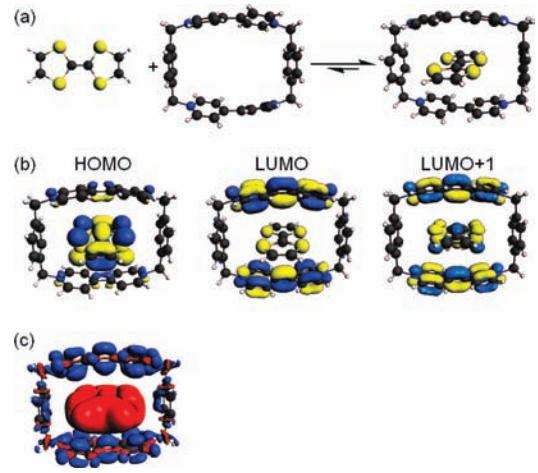

Figure 3. Representations of (a) the optimized geometries of TTF, $CBPQT^{4+}$, and TTF⊂ $CBPQT^{4+}$, (b) the frontier MOs of the complex, and (c) the change in the electronic distribution occurring during complexation (red = loss, blue = gain of electron density).

Calculated Geometries of TTF, $CBPQT^{4+}$, and the Complex TTF⊂$CBPQT^{4+}$. The geometries (Figures 3 and 4) of the individual components, TTF and $CBPQT^{4+}$, as well as of the TTF⊂$CBPQT^{4+}$ complex were modeled (Supporting Information) using density functional theory (DFT). All calculations were conducted using a local version of the Amsterdam density functional (ADF) program package.[44] The Becke−Perdew (BP86) XC-potential and a triple-ζ-polarized Slater-type (TZP) basis set from the ADF basis set library have been used. The 1s core has been kept frozen for C, N, and O atoms, and the 1s−2p core has been kept frozen for S. In agreement with previous studies, we find the gas-phase TTF to be in a boat conformation[45] and gas-phase $CBPQT^{4+}$ to have a small dihedral angle between the two pyridinium rings of each paraquat subunit.[46] The energy differences between the planar and nonplanar conformations are very small and within computational error for both uncomplexed units: <2 kcal mol^{-1}. On account of the fact that the experimental Raman spectrum of TTF was recorded herein in the solid state, we also optimized the planar structure constrained to have D_{2h} symmetry. This structure was then used to simulate the Raman spectrum of TTF.

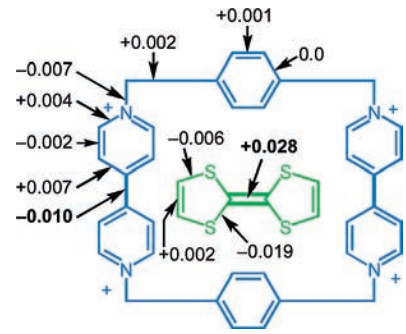

Figure 4. Computed bond length changes (angstroms) that occur upon complex formation. The largest changes occur in the bond lengths highlighted in bold.

Upon complexation, both of the components are planar, thus indicating a shift in the conformational preferences. The gas-phase binding energy is calculated to be −14.7 kcal mol^{-1} and is dominated by the orbital interaction. This is in good agreement[47] with the CT interactions in the complex where 0.46e$^-$ is transferred from TTF to $CBPQT^{4+}$. We obtained the

amount of CT by calculating the Voronoi deformation density charges,[48] which correspond to how much electronic charge enters or leaves a region of space around the nucleus arising from the redistribution of charge density that occurs upon forming the complex.

The HOMO of the complex (Figure 3b) shows some degree of mixing: 73% of the HOMO resides on the TTF unit and 24% resides on the LUMO+1 of $CBPQT^{4+}$, whereas the LUMO of the complex predominantly consists of the LUMO of the $CBPQT^{4+}$. As a consequence of this orbital mixing, the central TTF C=C bond lengthens significantly from 1.359 to 1.388 Å. The shortening of the C−S bonds and the lengthening of the terminal C=C bonds occur but to a smaller extent (Figure 4). These changes are consistent with the partial oxidation of the TTF unit upon complexation. In the fully oxidized TTF^{2+} dication, the bond length of the central C−C bond is calculated to be 1.456 Å. If we assume a linear change in the bond length as a function of the oxidation, a bond length of 1.388 Å found for the complexed TTF unit would indicate a partial oxidation of $0.6e^-$. This value is in good agreement with the $0.46e^-$ obtained in the Voronoi deformation density analysis. Similar changes are observed in the crystal structure of TTF^{2+}.[41] Within $CBPQT^{4+}$, the interpyridinium bond shortens from 1.492 to 1.481 Å, and the other pyridinium bonds display smaller changes, whereas the phenylene bond lengths remain relatively unaltered.

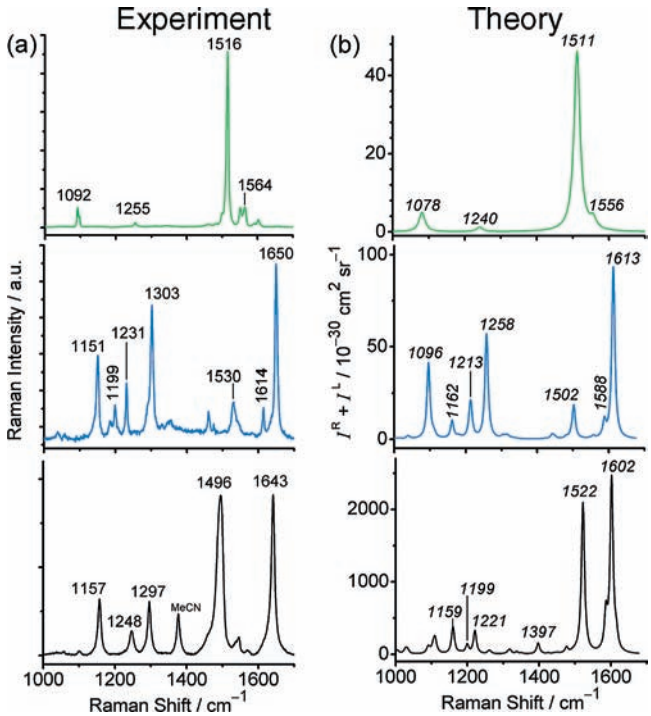

Figure 5. Experimental and calculated Raman spectra for (a) TTF (exptl: solid state; calcd: gas phase, D_{2h}), (b) $CBPQT^{4+}$ (exptl: $4PF_6^-$ salt in solid state; calcd: gas phase), and (c) the resonance Raman spectrum of the TTF⊂$CBPQT^{4+}$ complex (exptl: 11.5 mM, MeCN, 785 nm; calcd: gas phase).

Computed Raman and Resonance Raman Spectra. The calculations of the normal Raman and RRS spectra were performed as a means to provide assignments of the RRS spectra and a description of the normal modes of vibration. The computations were conducted using a recently developed time-dependent density functional theory (TDDFT) method, which uses a short-time approximation to evaluate the Raman scattering cross sections.[49] This approach neglects vibronic coupling effects on the RRS intensities;[24,29] however, they are expected to be small for the CT transition considered here. The finite lifetime of the excited state, which is needed for calculating the resonance Raman cross sections, is expressed by a common damping parameter ($\Gamma = 0.1$ eV). The spectra were calculated with $\lambda_{exc} = 850$ nm on the basis of scattering factors calculated on resonance with the CT transition. See the Supporting Information for full computational details. All spectra are unscaled. All computed vibrational band positions are italicized throughout the text.

The normal Raman spectra of the components show good correlations (Figure 5) to the experimental spectra in both position and intensity in the region above 1000 cm^{-1}. However, in the low wavenumber region, we see poorer agreement most likely arising from the neglect of solvent effects as well as anharmonic corrections. (See the Supporting Information.) The Raman scattering cross section is calculated to be about two times larger for $CBPQT^{4+}$ than TTF, which is consistent with observations (2×). The RRS spectra of the complex also show good correlations above 1000 cm^{-1}, even though the TDDFT method underestimated the CT transition energy by 0.6 eV.[47] Again, we find that the agreement is worse in the low-frequency range because of the neglect of solvent and vibronic effects.[7,9] It is well known that TDDFT underestimates CT excitations in weakly interacting systems because of a self-interaction error caused by the approximate XC functionals.[50] A correct description of the CT excitation in $CBPQT^{4+}$ complexes can be obtained using newer functionals as recently shown[51] for a [2]pseudorotaxene based on $CBPQT^{4+}$ using the M06-class of functionals.[52] However, in the RRS calculations, it is more important to describe correctly the curvature of the excited state in the Franck−Condon region than the actual energy position. Therefore, even though the CT transition is underestimated, the good agreement between the simulated and experimental RRS spectra for the complex provides a solid base for a detailed comparison. In general, there is a better agreement between the calculated and experimental vibrational frequencies for TTF than for both $CBPQT^{4+}$ and the complex. This is most likely due to the neglect of solvent effects and counterions in the calculations on the two tetracationic species.

The close agreement between the Raman spectra of all three systems provides a basis to assign the observed bands to the associated normal modes of vibration. We aided the assignments

TABLE 2: Selected Band Positions of TTF, $CBPQT^{4+}$, and the Complex in the Region above 1000 cm^{-1} from Experiment and Theory Together with the Band Assignments

TTF		$CBPQT^{4+}$		complex		
exptl[a]	*calcd*[b]	exptl[c]	*calcd*[d]	exptl[e]	*calcd*[d]	assign.
		1650	*1613*	1643	*1602*	$CBPQT^{4+}$
		1614	*1588*			$CBPQT^{4+}$
1564	*1556*			1496	*1522*	TTF
		1530	*1502*			$CBPQT^{4+}$
1516	*1511*				*1397*	TTF
		1303	*1258*			$CBPQT^{4+}$
1255	*1240*				*1221*	TTF
		1231	*1213*	1297	*1199*	$CBPQT^{4+}$
				1248	*1159*	$CBPQT^{4+}$
		1199	*1162*	1157		$CBPQT^{4+}$
		1151	*1096*			$CBPQT^{4+}$
1092	*1078*					TTF

[a] Solid state. [b] D_{2h}. [c] $CBPQT \cdot 4PF_6$ solid state. [d] Gas phase. [e] Solution (MeCN).

(Table 2) of the vibrations in the complex by calculating the overlap between the normal modes of the complex and the normal modes of TTF and of $CBPQT^{4+}$ (Supporting Information). All of the most intensely enhanced bands in the region above 1000 cm^{-1} are assigned to the complexed $CBPQT^{4+}$ unit with the exception of the band at *1522* cm^{-1}, which is assigned to the complexed TTF unit.

Both the observed and computed Raman spectra show small changes in the band positions upon complexation. The magnitudes of the shifts are consistent with the weak character of the noncovalent CT interactions, the fact that the interaction is distributed over six ring systems, and the small conformational changes. In situations when the normal modes do not change upon complexation, the shifts can be correlated[53] to changes in the bond order(s) of the constituent internal modes. On the basis of the modest changes in structure, it is reasonable to assume that each of the normal mode descriptions remains largely unaltered upon complexation. Whereas the majority of the changes in the normal mode descriptions are computed to be small, others are large.

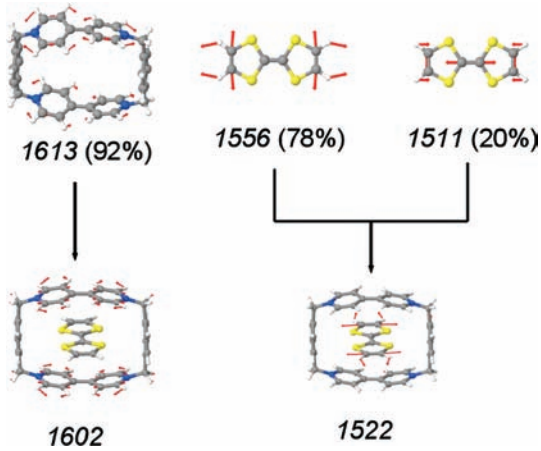

Figure 6. Representations of the most enhanced normal modes (cm^{-1}) for the complex and their mode compositions (%) based on the free components.

The bands that show the largest shifts toward lower wavenumber in the RRS spectra of the complex occur in the resonantly enhanced bands for $CBPQT^{4+}$ at 1643 cm^{-1} and TTF at 1496 cm^{-1}. The shift of the $CBPQT^{4+}$ band (1650 → 1643 cm^{-1}) is reproduced by computation (*1613* → *1602* cm^{-1}). The vibration-overlap calculations show (Table S1 in the Supporting Information) that the mode of the complex at *1602* cm^{-1} corresponds to 92% of the mode at *1613* cm^{-1} of the free $CBPQT^{4+}$ (Figure 6). This is a small perturbation in the mode description. Consequently, it is reasonable to ascribe the ∼10 cm^{-1} shift of the $CBPQT^{4+}$ band to a weakening of the constituent force constants originating from the mixing in the ground state between the HOMO and LUMO+1 (Figure 3b).

In contrast, the intense band assigned to the TTF unit computed at *1522* cm^{-1} shows large changes (Figure 6) in its normal mode description upon complexation. This TTF-localized mode of the complex corresponds to an admixture (Figure 6) of modes from the uncomplexed D_{2h}-TTF at *1511* (20%) and *1556* (78%) cm^{-1}. Even though the *1511* cm^{-1} band of the free TTF is the most intense (Figure 5), its contribution to the *1522* cm^{-1} band of the TTF⊂$CBPQT^{4+}$ complex is relatively small! Second, the normal mode for the *1522* cm^{-1} band of the complex no longer involves the internal mode of the central C═C bond of TTF. This internal mode is now associated with the weakly enhanced vibration at *1397* cm^{-1} (Supporting Information). Similarly, both large and small changes are seen to occur in the normal mode descriptions for the bands in the ∼1100−1300 cm^{-1} region when comparing the complex with the free $CBPQT^{4+}$ unit. The theoretical analysis shows that the same sets of internal modes are involved in the new normal modes and that their relative contributions have been redistributed. Taken together, these examples illustrate the care required in vibrational band assignments when interpreting shifts in band positions of the host, the guest, and the resulting complex.

The observation of resonance enhancement is consistent with complexation resulting from a CT interaction. The new CT electronic transition at 865 nm is calculated to occur between the TTF-HOMO and $CBPQT^{4+}$-LUMO orbitals of the complex. Because the RRS spectrum is obtained in resonance with this transition, we expect and observe vibrations that are modulated by charge redistributions in these π orbitals to be strongly enhanced. These modes correspond to in-plane vibrations of the paraquat subunits of $CBPQT^{4+}$ and the TTF unit that lie above 1000 cm^{-1}.

TABLE 3: SEF Values (λ_{exc} = 785 nm) Calculated for the Strong Bands Observed in the RRS Spectrum of TTF⊂$CBPQT^{4+}$

ν_{exptl} (cm^{-1})	SEF_{exptl}	ν_{calcd} (cm^{-1})	SEF_{calcd}	
1157	26	*1159*	38	$CBPQT^{4+}$
1248		*1199*	7	$CBPQT^{4+}$
1297	12	*1231*	6	$CBPQT^{4+}$
1496	33	*1522*	50	TTF
1643	31	*1602*	27	$CBPQT^{4+}$

Spectral enhancement factors (SEFs, Table 3) represent the intensity increases that arise from resonance when comparing the spectrum of the complex to the spectra of the individual host and guest components. The SEFs show reasonable correlations between experiment and theory. The fact that the normal mode descriptions have changed upon complexation for some of the bands means that these SEFs are merely phenomenological in nature and their relation to resonance enhancement factors should be qualified on a case-by-case basis. For instance, the SEFs for the experimental 1494 cm^{-1} and computed *1522* cm^{-1} bands represent both changes in normal mode descriptions as well as any resonance effects.

TABLE 4: RREF Values (λ_{exc} = 785 nm) Calculated for the Strong Bands Observed in the RRS Spectra of TTF⊂$CBPQT^{4+}$

ν_{exptl} (cm^{-1})	$RREF_{exptl}$	
1157	47	$CBPQT^{4+}$
1248		$CBPQT^{4+}$
1297	46	$CBPQT^{4+}$
1496	204	TTF
1643	96	$CBPQT^{4+}$

The resonance Raman enhancement factors (RREFs, Table 4) calculated by comparison of the Raman spectra recorded off-resonance (λ_{exc} = 514.5 nm) with the resonant spectra (λ_{exc} = 785 nm) reflect the structural distortions in the Franck−Condon excited state.[20] These enhancements derive from the depopulation of the TTF-based HOMO and the $CBPQT^{4+}$-based LUMO, leading to the excited-state electronic configuration $[CBPQT^{3+}\cdot TTF^{+}]^*$. For example, the TTF-based HOMO shows bonding character across each of the three C═C bonds. Consequently, the RRS shows the normal mode at *1522* cm^{-1},

which involves two of the three C═C bonds, to be one of the most resonantly enhanced vibrations.

Conclusions

The application of RRS to measure accurately the strength of a host−guest complexation between the TTF donor and the $CBPQT^{4+}$ acceptor has been successfully demonstrated. The calculated geometry change upon complexation reflects the $0.46e^-$ charge transfer and orbital mixing that occurs in the ground state. Good agreements between the experimental and computational Raman spectra of the components and of the complex were obtained showing both large and small changes in the normal modes upon complexation. This study provides a basis for extending Raman spectroscopy to other CT complexes in solution and to binding events localized at the surfaces of plasmonically active Ag or Au nanostructures using SERS.

Acknowledgment. A.H.F. thanks Indiana University for financial support. L.J. acknowledges funds and the Research Computing and Cyberinfrastructure from The Pennsylvania State University. J.O.J. thanks the Strategic Research Council in Denmark (project no. 2117-05-0115) for financial support.

Supporting Information Available: Experimental procedures for Raman spectroscopy measurements; normal Raman spectra of TTF and $CBPQT \cdot 4PF_6$; optimized structures, normal modes, and full calculated spectra of TTF, $CBPQT^{4+}$, and the $TTF \subset CBPQT^{4+}$ complex; determination of spectral and resonance Raman enhancement factors. This material is available free of charge via the Internet at http://pubs.acs.org.

References and Notes

(1) (a) Grynkiewicz, G.; Poenie, M.; Tsien, R. Y. *J. Biol. Chem.* **1985**, *260*, 3440–3450. (b) McQuade, D. T.; Pullen, A. E.; Swager, T. M. *Chem. Rev.* **2000**, *100*, 2537–2574. (c) Anslyn, E. V. *J. Org. Chem.* **2007**, *72*, 687–699. (d) Wansapura, C. M.; Seliskar, C. J.; Heineman, W. R. *Anal. Chem.* **2007**, *79*, 5594–5600.

(2) Lehn, J. M. *Supramolecular Chemistry: Concepts and Perspectives*; VCH: Weinheim, Germany, 1995.

(3) Kauffman, D. R.; Star, A. *Chem. Soc. Rev.* **2008**, *37*, 1197–1206.

(4) Jeanmaire, D. L.; Van Duyne, R. P. *J. Electroanal. Chem.* **1977**, *84*, 1–20.

(5) (a) Tolaieb, B.; Constantino, C. J. L.; Aroca, R. F. *Analyst* **2004**, *129*, 337–341. (b) Dieringer, J. A.; McFarland, A. D.; Shah, N. C.; Stuart, D. A.; Whitney, A. V.; Yonzon, C. R.; Young, M. A.; Zhang, X. Y.; Van Duyne, R. P. *Faraday Discuss.* **2006**, *132*, 9–26. (c) Bell, S. E. J.; Sirimuthu, N. M. S. *Chem. Soc. Rev.* **2008**, *37*, 1012–1024.

(6) Quantitative SERS examples: (a) McGlashen, M. L.; Davis, K. L.; Morris, M. D. *Anal. Chem.* **1990**, *62*, 846–849. (b) Carron, K.; Mullen, K.; Lanouette, M.; Angersbach, H. *Appl. Spectrosc.* **1991**, *45*, 420–423. (c) Carron, K.; Peltersen, L.; Lewis, M. *Environ. Sci. Technol.* **1992**, *26*, 1950–1954. (d) Heynes, J. B.; Sears, L. M.; Corcoran, R. C.; Carron, K. *Anal. Chem.* **1994**, *66*, 1572–1574. (e) Crane, L. G.; Wang, D.; Sears, L. M.; Heynes, J. B.; Carron, K. *Anal. Chem.* **1995**, *67*, 360–364. (f) Hill, W.; Wehling, B.; Gibbs, C. G.; Gutsche, C. D.; Klockow, D. *Anal. Chem.* **1995**, *67*, 3187–3192. (g) Teiten, B.; Burneau, A. *J. Raman Spectrosc.* **1997**, *28*, 879–884. (h) Hill, W.; Fallourd, V.; Klockow, D. *J. Phys. Chem. B* **1999**, *103*, 4707–4713. (i) Kanayama, N.; Kanbara, T.; Kitano, H. *J. Phys. Chem. B* **2000**, *104*, 271–278. (j) Uibel, R. H.; Harris, J. M. *Appl. Spectrosc.* **2000**, *54*, 1868–1875. (k) Marenco, C.; Stirling, C. J. M.; Yarwood, J. *J. Raman Spectrosc.* **2001**, *32*, 183–194. (l) Mosier-Boss, P. A.; Lieberman, S. H. *Appl. Spectrosc.* **2003**, *57*, 1129–1137.

(7) Qualitative SERS examples: (a) Maeda, Y.; Kitano, H. *J. Phys. Chem.* **1995**, *99*, 487–488. (b) Kanayama, N.; Kitano, H. *Langmuir* **2000**, *16*, 577–583. (c) Wei, A.; Kim, B.; Sadtler, B.; Tripp, S. L. *ChemPhysChem* **2001**, 743–745. (d) Alaverdian, I. S.; Feofanov, A. V.; Gromov, S. P.; Vedernikov, A. I.; Lobova, N. A.; Alfimov, M. V. *J. Phys. Chem. A* **2003**, *107*, 9542–9546. (e) Alaverdyan, Y. S.; Feofanov, A. V.; Gromov, S. P.; Vedernikov, A. I.; Lobova, N. A.; Alfimov, M. V. *Opt. Spectrosc.* **2004**, *97*, 560–566. (f) Leyton, P.; Sanchez-Cortes, S.; Garcia-Ramos, J. V.; Domingo, C.; Campos-Vallette, M.; Saitz, C.; Clavijo, R. E. *J. Phys. Chem. B* **2004**, *108*, 17484–17490. (g) Mosier-Boss, P. A. *Appl. Spectrosc.* **2006**, *60*, 1148–1156. (h) Guerrini, L.; Garcia-Ramos, J. V.; Domingo, C.; Sanchez-Cortes, S. *Phys. Chem. Chem. Phys.* **2009**, *11*, 1797–1793.

(8) (a) de Silva, A. P.; Gunaratne, H. Q. N.; Gunnlaugsson, T.; Huxley, A. J. M.; McCoy, C. P.; Rademacher, J. T.; Rice, T. E. *Chem. Rev.* **1997**, *97*, 1515–1556. (b) Yang, J. S.; Swager, T. M. *J. Am. Chem. Soc.* **1998**, *120*, 5321–5322. (c) Metzger, A.; Anslyn, E. V. *Angew. Chem., Int. Ed.* **1998**, *37*, 649–652. (d) Jiang, X.; Vieweger, M. C.; Bollinger, J. C.; Dragnea, B.; Lee, D. *Org. Lett.* **2007**, *9*, 3579–3852. (e) Staneva, D.; Grabchev, I.; Soumillion, J. P.; Bojinov, V. *J. Photochem. Photobiol., A* **2007**, *189*, 192–197. (f) Uchiyama, S.; Iwai, K.; de Silva, A. P. *Angew. Chem., Int. Ed.* **2008**, *47*, 4667–4669.

(9) Heterodimerization: Michaelian, K. H.; Rieckhoff, K. E.; Voigt, E. M. *J. Phys. Chem.* **1977**, *81*, 1489–1492.

(10) Metal-ligand binding: Hard, A. P.; Jayasooriya, U. A.; Cammidge, A. N. *Analyst* **2003**, *128*, 70–74.

(11) Use of Raman scattering for structural and electronic studies: (a) Michaelian, K. H.; Rieckhoff, K. E.; Voigt, E. M. *Chem. Phys. Lett.* **1973**, *23*, 5–8. (b) Michaelian, K. H.; Rieckhoff, K. E.; Voigt, E. M. *Proc. Natl. Acad. Sci. U.S.A.* **1975**, *72*, 4196–4199. (c) Michaelian, K. H.; Rieckhoff, K. E.; Voigt, E. M. *Chem. Phys. Lett.* **1976**, *39*, 521–524. (d) Michaelian, K. H.; Rieckhoff, K. E.; Voigt, E. M. *Chem. Phys. Lett.* **1983**, *99*, 512–514. (e) Shelnut, J. A. *Inorg. Chem.* **1983**, *22*, 2535–2544. (f) Shelnutt, J. A. *J. Am. Chem. Soc.* **1983**, *105*, 774–778. (g) Blackbourn, R. L.; Johnson, C. S.; Hupp, J. T.; Bryant, M. A.; Sobocinski, R. L.; Pemberton, J. E. *J. Phys. Chem.* **1991**, *95*, 10535–10537. (h) Markel, F.; Ferris, N. S.; Gould, I. R.; Myers, A. B. *J. Am. Chem. Soc.* **1992**, *114*, 6208–6219. (i) Benniston, A. C.; Harriman, A. *J. Am. Chem. Soc.* **1994**, *116*, 11531–11537. (j) Moreira, W. C.; Dutton, P. J.; Aroca, R. *Langmuir* **1995**, *11*, 3137–3144. (k) Kulinowski, K.; Gould, I. R.; Myers, A. B. *J. Phys. Chem.* **1995**, *99*, 9017–9026. (l) Kulinowski, K.; Gould, I. R.; Ferris, N. S.; Myers, A. B. *J. Phys. Chem.* **1995**, *99*, 17715–17723. (m) Paci, B.; Amoretti, G.; Arduini, G.; Ruani, G.; Shinkai, S.; Suzuki, T. *Phys. Rev. B* **1997**, *55*, 5566–5569. (n) Egolf, D. S.; Waterland, M. R.; Kelley, A. M. *J. Phys. Chem. B* **2000**, *104*, 10727–10737. (o) Cavagnat, D.; Brotin, T.; Bruneel, J. L.; Dutasta, J. P.; Thozet, A.; Perrin, M.; Guillaume, F. *J. Phys. Chem. B* **2004**, *108*, 5572–5581. (p) Phillips, D. L.; Gould, I. R.; Verhoeven, J. W.; TittelbachHelmrich, D.; Myers, A. B. *Chem. Phys. Lett.* **1996**, *258*, 87–93. (q) Kustner, B.; Schmuck, C.; Wich, P.; Jehn, C.; Srivastava, S. K.; Schlucker, S. *Phys. Chem. Chem. Phys.* **2007**, *9*, 4598–4603. (r) Pereira, C. C. L.; Nolasco, M.; Braga, S. S.; Almeida Paz, F. A.; Ribeiro-Claro, P.; Pillinger, M.; Goncalves, I. S. *Organometallics* **2007**, *26*, 4220–4228. (s) Blanch, G. P.; Del Castillo, M. L. R.; Del Mar Caja, M.; Perez-Mendez, M.; Sanchez-Cortes, S. *Food Chem.* **2007**, *105*, 1335–1341. (t) Pellegrin, Y.; Forster, R. J.; Keyes, T. E. *Inorg. Chim. Acta* **2008**, *361*, 2683–2691. (u) Srivastava, S. K.; Niebling, S.; Kustner, B.; Wich, P. R.; Schmuck, C.; Schlucker, S. *Phys. Chem. Chem. Phys.* **2008**, *10*, 6770–6775.

(12) (a) Hirose, K. In *Analytical Methods in Supramolecular Chemistry*; Schalley, C. A., Ed.; Wiley-VCH: Weinheim, Germany, 2007. (b) Li, Y.; Vander Griend, D. A.; Flood, A. H. *Supramol. Chem.* **2009**, *21*, 111–117.

(13) Aroca, R. *Surface-Enhanced Vibrational Spectroscopy*; Wiley: New York, 2006.

(14) We estimate that 1 mM would be a reasonable lower limit. Higher laser powers and longer acquisition times would extend this range further if required.

(15) Saito, S.; Tasami, M.; Eugster, C. H. *J. Raman Spectrosc.* **1983**, *14*, 299–309.

(16) The higher concentrations (50 mM) for the TCNE heterodimers stem from their weak affinities ($K_a < 20\ M^{-1}$).

(17) (a) Baker, G. A.; Moore, D. S. *Anal. Bioanal. Chem.* **2005**, *382*, 1751–1770. (b) Willets, K. A.; Van Duyne, R. P. *Annu. Rev. Phys. Chem.* **2007**, *58*, 627–697. (c) Stiles, P. L.; Dieringer, J. A.; Shah, N. C.; Van Duyne, R. P. *Annu. Rev. Anal. Chem.* **2008**, *1*, 601–626.

(18) Reipa, V.; Laura Yeh, S.-M.; Monbouquette, H. G.; Vilker, V. L. *Langmuir* **1999**, *15*, 8126–8132.

(19) (a) Kitagawa, T.; Ozaki, Y.; Teraoka, J.; Kyogoku, Y.; Yamanaka, T. *Biochim. Biophys. Acta* **1977**, *494*, 100–114. (b) Spiro, T. G.; Ramsden, J. *Biochemistry* **1989**, *28*, 3125–3128.

(20) (a) Hirakawa, A. Y.; Tsuboi, M. *Science* **1975**, *188*, 359–361. (b) Myers, A. B.; Mathis, R. A. In *Biological Applications of Raman Spectroscopy*; Spiro, T. G., Ed.; Wiley: New York, 1987; Vol. 2H.

(21) (a) Markel, F.; Ferris, N. S.; Gould, I. R.; Myers, A. B. *J. Am. Chem. Soc.* **1992**, *114*, 6208–6219. (b) Kulinowski, K.; Gould, I. R.; Myers, A. B. *J. Phys. Chem.* **1995**, *99*, 9017–9026. (c) Lilichenko, M.; Verhoeven, J. W.; Myers, A. B. *Spectrochim. Acta, Part A* **1997**, *53*, 2079–2093.

(22) Shelnut, J. A. *J. Phys. Chem.* **1983**, *87*, 605–616.

(23) Neugebauer, J.; Hess, B. A. *J. Chem. Phys.* **2004**, *120*, 11564–11577.

(24) Guthmuller, J.; Champagne, B. *J. Chem. Phys.* **2007**, *127*, 164507.

(25) Peticolas, W. L.; Rush, T., III. *J. Comput. Chem.* **1995**, *16*, 1261–1270.

(26) Mennucci, B.; Cappelli, C.; Cammi, R.; Tomasi, J. *Theor. Chem. Acc.* **2007**, *117*, 1029–1039.

(27) Jarzecki, A. *J. Phys. Chem. A* **2009**, *113*, 2926–2934.

(28) Petrenko, T.; Neese, F. *J. Chem. Phys.* **2007**, *127*, 164319.
(29) Kiewisch, K.; Neugebauer, J.; Reiher, M. *J. Chem. Phys.* **2008**, *129*, 204103.
(30) Albrecht, A. C. *J. Chem. Phys.* **1961**, *34*, 1476–1484.
(31) Champion, P. M.; Albrecht, A. C. *Annu. Rev. Phys. Chem.* **1982**, *33*, 353–376.
(32) Heller, E. J.; Sundberg, R. L.; Tannor, D. *J. Phys. Chem.* **1982**, *86*, 1822–1833.
(33) Tannor, D. J.; Heller, E. J. *J. Chem. Phys.* **1982**, *77*, 202–218.
(34) Meyers, A. B. *Chem. Rev.* **1996**, *96*, 911–926.
(35) (a) Bryce, M. R. *J. Mater. Chem.* **2000**, *10*, 589–598. (b) Segura, J. L.; Martín, N. *Angew. Chem.* **2001**, *113*, 1416–1455. (c) Segura, J. L.; Martín, N. *Angew. Chem., Int. Ed.* **2001**, *40*, 1372–1409. (d) Schukat, G.; Fanghänel, E. *Sulfur Rep.* **2003**, *24*, 1–282. (e) Becher, J.; Jeppesen, J. O.; Nielsen, K. *Synth. Met.* **2003**, *133*−*134*, 309–315. (f) Jeppesen, J. O.; Becher, J. *Eur. J. Org. Chem.* **2003**, 3245–3266. (g) *TTF Chemistry*; Yamada, J.-I., Sugimoto, T., Eds.; Kodansha: Tokyo, Japan, 2004. (h) See the special issue on Molecular Conductors: *Chem. Rev* **2004**, *104*, 4887−5782. (i) Otsubo, T.; Takimiya, K. *Bull. Chem. Soc. Jpn.* **2004**, *77*, 43–58.
(36) (a) Anelli, P. L.; Ashton, P. R.; Ballardini, R.; Balzani, V.; Delgado, M.; Gandolfi, M. T.; Goodnow, T. T.; Kaifer, A. E.; Philp, D.; Pietraszkiewicz, M.; Prodi, L.; Reddington, M. V.; Slawin, A. M. Z.; Spencer, N.; Stoddart, J. F.; Vicent, C.; Williams, D. J. *J. Am. Chem. Soc.* **1992**, *114*, 193–218. (b) Asakawa, M.; Dehaen, W.; L'abbé, G.; Menzer, S.; Nouwen, J.; Raymo, F. M.; Stoddart, J. F.; Williams, D. J. *J. Org. Chem.* **1996**, *61*, 9591–9595.
(37) (a) Philp, D.; Slawin, A. M. Z.; Spencer, N.; Stoddart, J. F.; Williams, D. J. *J. Chem. Soc., Chem. Commun.* **1991**, 1584–1586. (b) Credi, A.; Montalti, M.; Balzani, V.; Langford, S. J.; Raymo, F. M.; Stoddart, J. F. *New. J. Chem.* **1998**, *22*, 1061–1065.
(38) Long, J. R.; Drago, R. S. *J. Chem. Educ.* **1982**, *59*, 1037–1039.
(39) (a) Lokey, R. S.; Iverson, B. L. *Nature* **1995**, *375*, 303–305. (b) Rathore, R.; Lindeman, S. V.; Kochi, J. K. *J. Am. Chem. Soc.* **1997**, *119*, 9393–9404. (c) Lee, J. W.; Kim, K.; Choi, S.; Ko, Y. H.; Sakamoto, S.; Yamaguchi, K.; Kim, K. *Chem. Commun.* **2002**, 2692–2693. (d) Kaiser, G.; Jarrosson, T.; Otto, S.; Ng, Y. F.; Bond, A. D.; Sanders, J. K. M. *Angew. Chem., Int. Ed.* **2004**, *43*, 1959–1962. (e) Nielsen, K. A.; Cho, W. S.; Jeppesen, J. O.; Lynch, V. M.; Becher, J.; Sessler, J. L. *J. Am. Chem. Soc.* **2004**, *126*, 16296–16297. (f) Gayathri, S. S.; Wielopolski, M.; Perez, E. M.; Fernandez, G.; Sanchez, L.; Viruela, R.; Orti, E.; Guldi, D. M.; Martín, N. *Angew. Chem., Int. Ed.* **2009**, *48*, 815–819. (g) Wang, R.; Liu, W.; Chen, Y.; Zuo, J. L.; You, X. Z. *Dyes Pigm.* **2009**, *1*, 40–44. (h) Li, W. Y.; Chen, X. F.; Xuan, C. S. *Spectrochim. Acta, Part A* **2009**, *71*, 1769–1775. (i) Asker, E.; Masnovi, J. *Spectrochim. Acta, Part A* **2009**, *71*, 1973–1978.
(40) Nygaard, S.; Hansen, S. W.; Huffman, J. C.; Jensen, F.; Flood, A. H.; Jeppesen, J. O. *J. Am. Chem. Soc.* **2007**, *129*, 7354–7363.
(41) Ashton, P. R.; Balzani, V.; Becher, J.; Credi, A.; Fyfe, M. C. T.; Mattersteig, G.; Menzer, S.; Nielsen, M. B.; Raymo, F. M.; Stoddart, J. F.; Venturi, M.; Williams, D. J. *J. Am. Chem. Soc.* **1999**, *121*, 3951–3957.
(42) Choi, J. W.; Flood, A. H.; Steuerman, D. W.; Nygaard, S.; Braunschweig, A. B.; Moonen, N. N. P.; Laursen, B. W.; Luo, Y.; DeIonno, E.; Peters, A. J.; Jeppesen, J. O.; Xu, K.; Stoddart, J. F.; Heath, J. R. *Chem.*−*Eur. J.* **2006**, *12*, 261–279.
(43) Vander Griend, D. A.; Bediako, D. K.; DeVries, M. J.; DeJong, N. A.; Heeringa, L. P. *Inorg. Chem.* **2008**, *47*, 656–662.
(44) (a) te Velde, G.; Bickelhaupt, F. M.; van Gisbergen, S. J. A.; Fonseca Guerra, C.; Baerends, E. J.; Snijders, J. G.; Ziegler, T. *J. Comput. Chem.* **2001**, *22*, 931–967. (b) *ADF*, local version; SCM, Theoretical Chemistry, Vrije Universiteit: Amsterdam, The Netherlands. www.scm.com.
(45) Ercolani, G.; Mencarelli, P. *J. Org. Chem.* **2003**, *68*, 6470–6473.
(46) Odell, B.; Reddington, M. V.; Slawin, A. M. Z.; Spencer, N.; Stoddart, J. F.; Williams, D. J. *Angew. Chem., Int. Ed. Engl.* **1988**, *11*, 1547–1550.
(47) (a) Jang, Y. H.; Hwang, S. G.; Kim, Y. H.; Jang, S. S.; Goddard, W. A. *J. Am. Chem. Soc.* **2004**, *126*, 12636–12645. (b) Deng, W. Q.; Flood, A. H.; Stoddart, J. F.; Goddard, W. A. *J. Am. Chem. Soc.* **2005**, *127*, 15994–15995.
(48) te Velde, G.; Bickelhaupt, F. M.; Baerends, E. J.; Fonseca Guerra, C.; van Gisbergen, S. J. A.; Snijders, J. G.; Ziegler, T. *J. Comput. Chem.* **2001**, *22*, 931–967.
(49) Jensen, L.; Zhao, L.; Autschbach, J.; Schatz, G. C. *J. Chem. Phys.* **2005**, *123*, 174110.
(50) Dreuw, A.; Weisman, J. L.; Head-Gordon, M. *J. Chem. Phys.* **2003**, *119*, 2943–2946.
(51) Benitez, D.; Tkatchouk, E.; Yoon, I.; Stoddart, J. F.; Goddard, W. A. *J. Am. Chem. Soc.* **2008**, *130*, 14928–14929.
(52) Zhao, Y.; Truhlar, D. G. *Acc. Chem. Res.* **2008**, *41*, 157–167.
(53) Matsuzaki, S.; Moriyama, T.; Toyoda, K. *Solid State Commun.* **1980**, *34*, 857–859.

JP905202X